Ionic size effect due to a nonclassical percolation process on the superconductor-insulator transition in $R_{1-x}Pr_xBa_2Cu_3O_{7-\delta}$ (R=rare earth)

Katsukuni Yoshida

Department of Fundamental Energy Science, Graduate School of Energy Science, Kyoto University, Uji, Kyoto 611-0011, Japan

(Received 8 December 2006; revised manuscript received 27 February 2007; published 23 July 2007)

The ionic size effect of rare earth R on the superconductor-insulator (S-I) transition in Pr-doped cuprates $R_{1-x}Pr_xBa_2Cu_3O_{7-\delta}$ (RPr-123) has been quantitatively investigated in terms of a nonclassical percolation process which includes two kinds of virtual percolation thresholds x_1 and x_2 originating from the classical percolation thresholds x_{pc1} and x_{pc2}. Such virtual thresholds take values different from those of the classical ones, and have been experimentally observed for YPr-123. The nonclassical percolation process is based on a mechanism where the crystal unit cell of R-123 changes when adjoining unit cells of Pr-123 into a different cell that behaves as if it were a Pr-123 cell. This cell conversion needs an assist from the $4f$(Pr)-$2p$(O) orbital hybridization, and creates the virtual threshold x_2 corresponding to the S-I transition point. The cell conversion advances more easily as the ionic size of R increases, giving rise to the size effect. The model gives quantitative results for the S-I transition depending on the ionic size in agreement with experimental observations for a variety of doped cuprates RPr-123. This nonclassical percolation process involving the cell conversion will also change the effective area of the antiferromagnetic ordering of the magnetic moments of Pr^{3+}.

DOI: 10.1103/PhysRevB.76.024514 PACS number(s): 74.72.Bk, 64.60.Ak, 74.62.Dh, 74.25.Fy

I. INTRODUCTION

In Pr-doped cuprates $R_{1-x}Pr_xBa_2Cu_3O_{7-\delta}$ (RPr-123), the ionic size of R (rare-earth elements) has been found to largely affect the superconductor-insulator (S-I) transition occurring when the Pr concentration x reaches a critical value, which decreases with increasing ionic size of R.[1–4] This size effect is coupled with the problem of how Pr doping deteriorates the superconductivity of $RBa_2Cu_3O_{7-\delta}$ (R-123). At present, this deterioration is believed to associate with the localization of holes around the dopant Pr, which is ascribable to the hybridization between Pr-4f orbital and neighboring O-2p orbital in the CuO_2 plane.[5–7] However, the comprehensive understanding of how the S-I transition occurs on increasing Pr concentration (x) and how the ionic size of R plays a role in determining the critical values for the S-I transition seems to be unestablished, in spite of a variety of explanations.[1,3,4,8,9] Most of such models have been based on the presumption that the doped cuprate RPr-123 is structurally homogeneous, where the change in the overall concentration of mobile holes or hole pairs has been a key issue for the explanation.

On the other hand, apart from the above line of thought, a variety of phenomena indicating that the dopant element such as Pr locally works in the cuprate have been observed; such as the disorder-induced localization of free carriers in YPr-123,[10] the flux pinning by dopant Pr giving an area of the locally lowered order parameter,[11,12] the percolative behavior of the electrical resistivity and the diamagnetism in doped cuprates, such as ErR-123, La-Pr-Ca-Ba-Cu-O, and YPr-123,[13–16] and a non-Ohmic resistance of RPr-123 as an increasing or decreasing function of the supplied current.[17,18] These observations indicate the presence of a nanostructural inhomogeneity introduced by dopant elements in the cuprates. In particular, the transport properties of Pr-doped cuprates have been found to reflect the percolation process and thereby the S-I transition can be determined by the percolation threshold.[14–16]

As described in a previous paper,[16] the doped cuprate $Y_{1-x}Pr_xBa_2Cu_3O_{7-\delta}$ (YPr-123) can be regarded as a mixed crystalline solid solution consisting of two kinds of crystal unit cells Y-123 (Y cell) and Pr-123 (Pr cell), where a two-dimensional (2D) site-percolation structure (square lattice) is built along the ab plane. Figure 1(a) depicts typical geometry of the conducting paths at low and high Pr concentrations x; the range is partitioned by the first site-percolation threshold $x_{pc1}=0.41$. On the lower concentration side ($x<x_{pc1}$), the

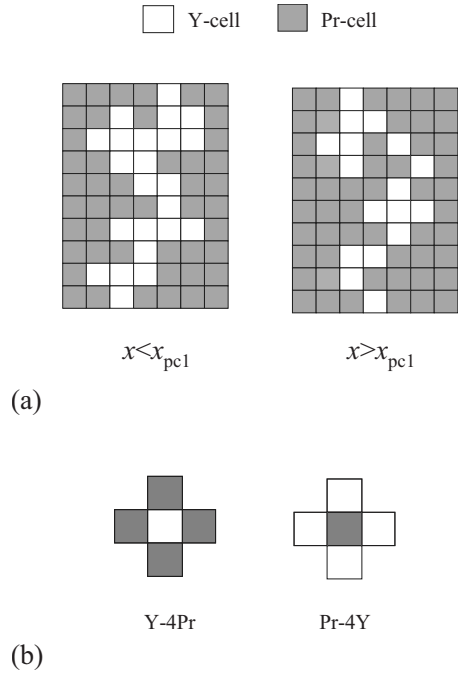

FIG. 1. (a) Percolative current path consisting of crystal unit cells of Y-123 (Y-cells) at Pr concentration x lower (type 1) than the threshold x_{pc1} or higher (type 2) than x_{pc1}, viewed from the c-axis direction (Ref. 16); (b) the configuration of cells when centered Y cell or Pr cell is converted (Y-4Pr, Pr-4Y).

conducting path is built with such Y cells as joining each other at their lateral faces (type 1), and on the higher concentration side ($x > x_{pc1}$), it changes into the path of type 2 built with Y cells joining each other at the corner of the adjacent cells in addition to the connection at lateral faces. The conducting path of type 2 is completely broken at x exceeding the second percolation threshold $x_{pc2}=0.59$, and its superconductivity is more fragile against the applied field than that of type 1.[16] The superconducting current is assumed to pass along these conducting paths consisting of Y cells, but be blocked by the Pr cell; here, the conduction is performed through the connection of the CuO_2 planes constituting Y cells. For this system, the diamagnetic susceptibility (χ) depending on the Pr concentration (x) has been found to exhibit characteristic points x_1 and x_2 which feature a percolation process, but their values shift a little from those of the classical percolation thresholds x_{pc1} and x_{pc2}. This variance indicates occurrence of a nonclassical percolation process, where a constituent crystal unit cell of Y-123 (or Pr-123) loses its electronic identity and can be converted into a different cell, when placed in a particular configuration of the cells, as depicted in Fig. 1(b).[16,19] Such cell conversion will be caused when the crystal unit cell of R-123 shares the electronic orbitals with the adjoining cells of different kind.

In the present study, after the percolative behavior of the χ-x curves for YPr-123 is experimentally demonstrated, its explanatory model will be elaborated in terms of the cell conversion with the aid of the $4f$-$2p$ hybridization, and further developed into a generalized form to quantitatively explain the size effect for a series of RPr-123 by determining the critical values at which the S-I transition takes place. In the model, the $4f$-$2p$ hybridization helps a R-123 cell (R cell) placed in a special configuration to convert into a different cell behaving as if it were a Pr-123 cell (Pr cell), and this conversion is assumed to take place more easily when the ionic size of R increases, where a variety of unit-cell configurations concern the cell conversion, according to the ionic size. By performing a mathematical formulation and computer simulations, this generalized percolation model is demonstrated to quantitatively determine the S-I transition points for the isostructural family of doped cuprates RPr-123. The purpose of this study is to elucidate the ionic size effect on the superconductor-insulator transition in terms of the nonclassical percolation process involving the unit-cell conversion of various types.

II. NONCLASSICAL PERCOLATION PROCESS IN YPr-123

First, let us show that the ac diamagnetic susceptibility (χ) demonstrates well how the superconducting current behaves in Pr-doped cuprates. As seen from the comparison of Figs. 2(a) and 2(b), after the overall superconductivity is realized at $T=T_0$ (zero-resistance temperature), the resistivity ρ gives no information more than the fact $\rho=0$, while χ tells behavior of the superconducting (diamagnetic) current for $T \leqslant T_0$. As seen from Fig. 2(b), at temperatures below T_0, the diamagnetic current reduces with increasing applied magnetic field h; the field h was applied by the ac current (1 kHz) supplied for measuring the inductance of the

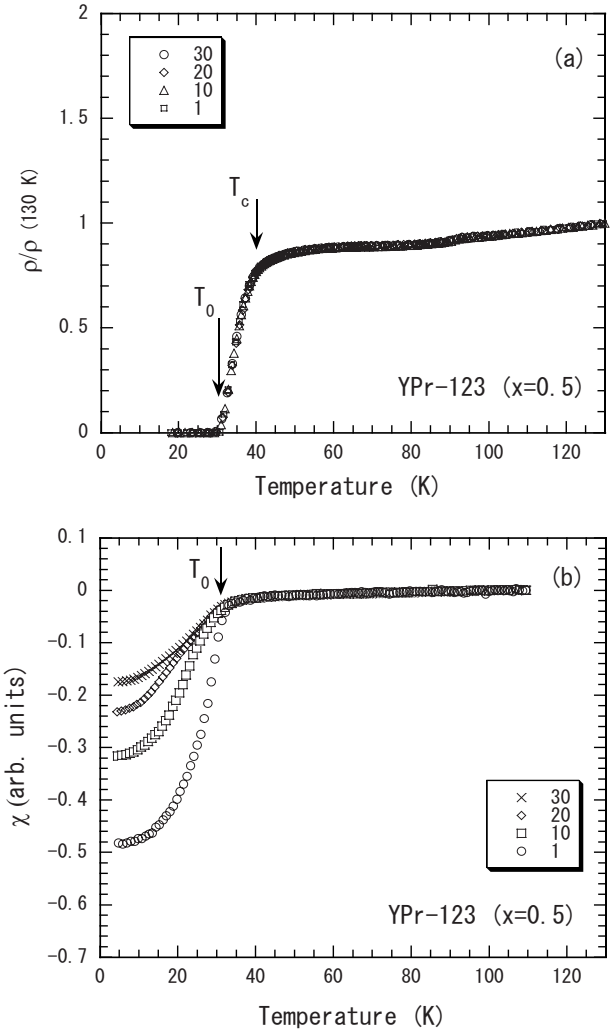

FIG. 2. Comparison between (a) the resistivity ρ and (b) the ac diamagnetic susceptibility χ (real part) of YPr-123 ($x=0.5$). T_c and T_0 indicate the onset and zero-resistance temperatures: (a) the legend figures (1, 10, 20, 30) refer to the dc current density (0.014, 0.14, 0.28, 0.42 A/cm^2), and (b) the legend figures (1, 10, 20, 30) refer to the intensity (rms) of ac magnetic field h (0.1, 1, 2, 3 Oe).

samples placed in a coil. It should be noticed that the onset temperature at which the curve of χ begins to steeply fall off just corresponds to the zero-resistance temperature T_0.[20] At around T_0, the superconducting path begins to complete a diamagnetic current loop passing throughout the medium, although the loop is strongly meandering, running near the sample surface in some parts and going inside apart from the surface in other parts. This situation refers to beginning of the zero resistance (i.e., the percolation transition), when the superconducting path is completed to pass throughout the sample. Figure 3 depicts the behavior of the ac diamagnetic susceptibility (real part) as a function of x. The samples used are polycrystalline ones and belong to the same series of samples (onset $T_c=93$ K for $x=0$) as reported previously;[16,21] they were prepared by the solid reaction method from a stoichiometric mixture of raw powders of Y_2O_3, Pr_6O_{11}, $BaCO_3$, and CuO. As exhibited in Fig. 3(a), the original percolation thresholds (classical) for the site-

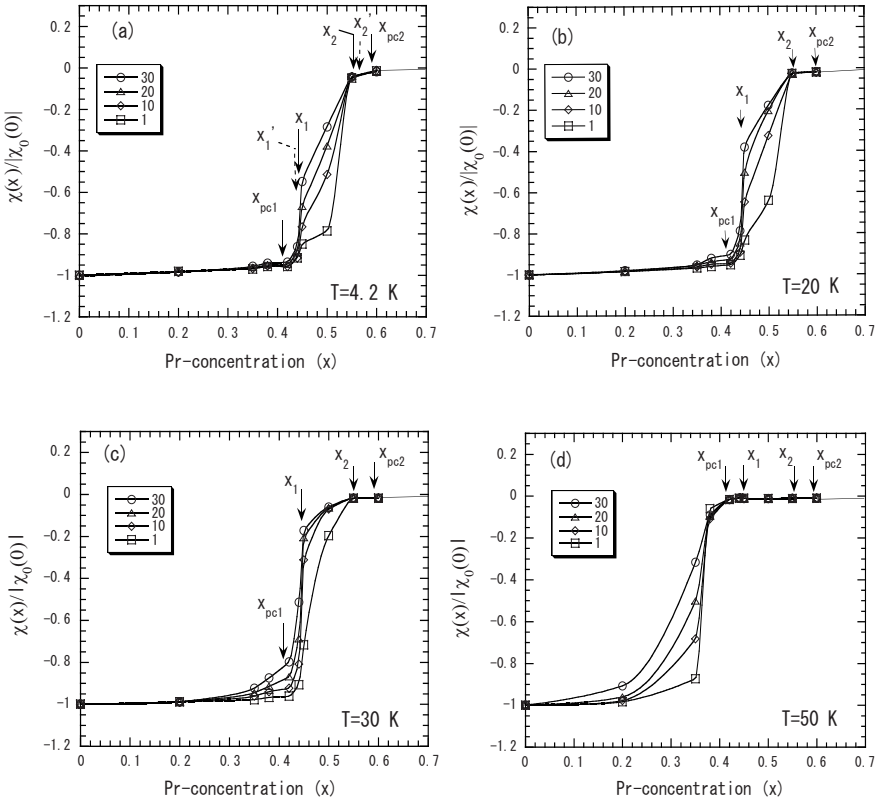

FIG. 3. Diamagnetic susceptibility χ (normalized with the absolute value at $x=0$ and $h=0.1$ Oe) as a function of Pr concentration x in YPr-123 at (a) $T=4.2$ K, (b) $T=20$ K, (c) $T=30$ K, and (d) $T=50$ K: the solid arrows indicate the original percolation thresholds x_{pc1} (first) and x_{pc2} (second), and corresponding virtual thresholds x_1 and x_2; the broken arrows (x_1' and x_2') indicate the estimation from Eq. (1); the legend figures (1, 10, 20, 30) indicate intensity (rms) of ac magnetic field h (0.1, 1, 2, 3 Oe); in the legends, each of the bars attached to the symbols merely indicates an eye-guiding passing through the experimental points (does not mean an error bar).

percolation system are indicated by the arrows at $x_{pc1}=0.41$ and $x_{pc2}=0.59$. However, the characteristic points where χ begins to dramatically vary are observed at different points $x_1 \simeq 0.44$ and $x_2 \simeq 0.55$. Noticeable is that the dependence of χ on the field h is considerable within the range between x_1 and x_2, implying that the superconducting path of type 2 [Fig. 1(a)] is constructed in this range, instead of the expected range between the original thresholds x_{pc1} and x_{pc2}.[16] As shown in Fig. 3(b), this behavior of χ remains almost invariant up to temperature as high as $T=20$ K. After then, with increasing T, the χ-x curves exhibit some deformation, but the characteristic points x_1 and x_2 still stand visible up to $T=30$ K [Fig. 3(c)]. Although not shown here, the point x_1 remains observable even at $T=40$ K, indicating that the conducting path of type 1 still survives as a superconducting path. At much higher temperatures, as shown in Fig. 3(d), the x_1 and x_2 submerge and the kink point merely shifts to the lower concentration side, implying that current path needs to be thicker for propagating the superconductivity than that needed at lower temperatures. The locations of x_1 and x_2 are almost independent of T and h at low temperatures below 20 K, implying that those points are inherent in the structure.

The occurrence of these characteristic points x_1 and x_2 will be explained by the following mechanism. As shown in Fig. 1(b), when an isolated Y cell adjoins four Pr cells at lateral faces (Y-4Pr), the O-2p orbitals in CuO_2 planes of the centered Y cell will be shared with the surrounding Pr cells. Then the orbitals ($2p_\pi$) of the oxygen ions common to Y and Pr cells will hybridize with the 4f orbitals stemming from the Pr cells, so that the centered Y cell (i.e., its CuO_2 planes) will lose the initial electronic identity, and therefore the existing hole will be trapped to become immobile by the effective hybridized orbitals. Then the centered Y cell behaves as if it were a Pr cell. In contrast, when an isolated Pr cell is surrounded by four Y cells [Pr-4Y in Fig. 1(b)], the O-2p orbitals in CuO_2 plane are shared with among them, and the 4f-2p hybridization initially realized in the centered Pr cell is released so that this Pr cell will also be converted into a different cell behaving as it were a Y cell. We consider that the latter assumption will be applicable only when R of the surrounding cells has no 4f orbital, or if it exists, its spatial extension is small, so that the initial 4f-2p hybridization originating from the centered Pr-123 cell may be released. The cell conversion makes a difference in counting of the cells as the structural units, so that the effective thresholds (x_1 and x_2) are shifted from the original ones (x_{pc1} and x_{pc2}), and the second threshold x_2 refers to the S-I transition;[16] from now on, x_1 and x_2 will often be referred to as virtual percolation thresholds.

Let us estimate what amount the percolation thresholds shift from the original ones. The concentrations of the isolated Y cells (Y-4Pr) and the isolated Pr cells (Pr-4Y) are, respectively, counted as $(1-x)x^4$ and $(1-x)^4x$ from the standard percolation theory.[22] These converted Y and Pr cells are counted as effective Pr and Y cells, respectively. Then the virtual percolation thresholds x_2 and x_1 will be approximately obtained from the following equation:

$$x + x^4(1-x) - x(1-x)^4 = x_{pc}, \tag{1}$$

where x_{pc} is the original percolation threshold $x_{pc1}(=0.41)$ or $x_{pc2}(=0.59)$. It should be noticed that the solutions of Eq. (1) only give approximation to the real values of x_2 and x_1, because the conversion of the cells induces incompleteness

TABLE I. Experimental and theoretical (simulated and calculated) values of thresholds x_2 and x_1 for RPr-123 with rare-earth ion R^{3+}; x_2 refers to the second percolation threshold (virtual) when the superconductivity disappears (S-I transition) and x_1 refers to the first percolation threshold (virtual): k_2's value with notation "$*$" refers to asymmetric configuration (R-2Pr-a).

Items	Class 1	Class 2	Class 3	Class 4
Ionic radius (Å) of R^{3+} (eightfold configuration)	Nd: 1.11	Eu: 1.07 Sm: 1.08	Gd: 1.05	Y: 1.02 Ho: 1.02 Dy: 1.03
Experimental x_2	Nd: 0.3–0.32[a–c]	Eu: 0.39–0.42[d,e] Sm: 0.35–0.4[k–m]	Gd: 0.45[f–h]	Y: 0.55[i,j] Ho: 0.57[n] Dy: 0.56[o]
Experimental x_1				Y: 0.44[i]
Simulated x_2	0.295	0.395	0.445	0.554
Simulated x_1	0.265	0.337	0.410	0.446
Calculated x_2	0.325	0.365	0.455	0.566
Calculated x_1	0.233	0.260	0.336	0.435
Configurations	R-4Pr,R-3Pr R-2Pr-a, R-2Pr-s	R-4Pr, R-3Pr R-2Pr-a	R-4Pr, R-3Pr	R-4Pr, Pr-4R
Coefficients k_n	$k_4=k_3=k_2=1$ $k_1=0$	$k_4=k_3=1$ $k_2=2/3^*$, $k_1=0$	$k_4=k_3=1$ $k_2=k_1=0$	$k_4=1$ and see Eq. (1) $k_3=k_2=k_1=0$

[a]Reference 18.
[b]Reference 25.
[c]Reference 26.
[d]Reference 30.
[e]Reference 31.
[f]Reference 17.
[g]Reference 27.
[h]Reference 28.
[i]Reference 16.
[j]Reference 29.
[k]Reference 4.
[l]Reference 32.
[m]Reference 33.
[n]Reference 23.
[o]Reference 24.

more or less in the structural randomness of the percolation system. The solutions of Eq. (1) give the following values for x_2 and x_1:

$$x_2 \approx 0.566, \quad x_1 \approx 0.435. \tag{2}$$

In Fig. 3(a), these calculated values are indicated by the broken arrows (x_2', x_1'), showing good approximation to the values observed.

More realistic values of x_1 and x_2 are obtained from simulations for the computer-generated site-percolation system on the square lattice by applying the cell conversions (Y-4Pr and Pr-4Y) together with the periodic boundary condition; the system employed here has dimensions $L^2=10^4$. The computer-simulated values are as follows:

$$x_2 \simeq 0.554, \quad x_1 \simeq 0.446. \tag{3}$$

As demonstrated in Fig. 3(a), the simulated values of x_1 and x_2 show better agreement with the experimental observations than those calculated from Eq. (1). As exhibited in Table I, the same result can also be adapted to other members such as $Ho_{1-x}Pr_xBa_2Cu_3O_{7-\delta}$ (HoPr-123) (Ref. 23) and $Dy_{1-x}Pr_xBa_2Cu_3O_{7-\delta}$ (DyPr-123) (Ref. 24); the elements Ho and Dy have 4f electrons, but have ionic sizes almost equal to that of Y (Table I).

The above results indicate that the filamentary current path as narrow as the width of the unit cell of Y cell, as depicted in Fig. 1(a), is capable of propagating the superconductivity, and hence that the hole pair has a space as small as the lattice constant (a or b). Therefore, it seems rather surprising that the coherent state of the superconductivity can be sustained in such a narrow path. However, it will be worth considering the following. The arrangement of Cu(2) spins, which contributes to realization of the superconductivity, is networked continuously over the CuO_2 lattice system embracing both of Y and Pr cells. Reflecting this spin lattice in common to both kinds of the cells, the superconducting state in such a narrow area might be sustained not only by direct contribution from the relevant Y cells on the narrow path but also mediated by a background of the Pr cells; however, this situation would not be realized unless two kinds of the unit cells are isostructural.

III. GENERALIZATION FOR *R*Pr-123 HAVING LARGER IONIC SIZE OF *R*

The model described so far, as it stands, is inapplicable to the case when the ionic size of R is larger than that of Y, because the S-I transition for such RPr-123 takes place at different values of x_2 ranging from 0.32 (for R=Nd) (Refs. 18 and 25) to 0.45 (for R=Gd),[17,27,28] which are noticeably

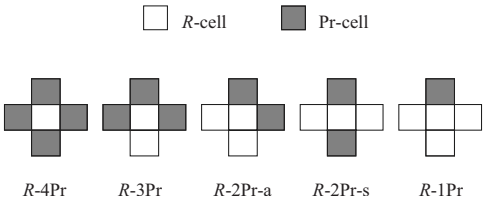

FIG. 4. Configurations (R-nPr) of unit cells for conversion of the centered cell R; R-2Pr has symmetric (R-2Pr-s) and asymmetric (R-2Pr-a) configurations.

smaller than that observed for YPr-123 (x_2=0.55).[16,29]

In order to develop the model into a more general form, we assume the following. Firstly, as the ionic size increases, the unit cell of R-123 (R-cell) can more easily be converted into a different cell behaving as if it were Pr cell, that is, adjoining Pr cells fewer than four [as depicted by Y-4Pr in Fig. 1(b)] can convert the centered R cell; secondly, for the reversed configuration [as depicted by Pr-4Y in Fig. 1(b)], the surrounding R cells cannot release the $4f$-$2p$ hybridization at the centered Pr cell, except when R is as small as that of Y or smaller. The above assumption implies the following view. As the ionic size of R increases, the largely extending $4f$ orbitals of R will hybridize more easily with $2p$ orbitals of the oxygen in cooperation with the neighboring $4f$ orbitals from the surrounding Pr ions. The cell configurations that cause the conversion of the centered R cell are shown in Fig. 4 with the number (n) of adjoining Pr cells: n=4 (R-4Pr), n=3 (R-3Pr), n=2 (R-2Pr), and n=1 (R-1Pr), where the configuration R-2Pr has two types that are asymmetric (R-2Pr-a) and symmetric (R-2Pr-s) and the population of R-2Pr-a doubles that of R-2Pr-s.

As stated above, the centered R cell is more easily converted by increasing the ionic size (radius) of R. Therefore, the number of the configuration types pertaining to the cell conversion increases stepwise with increasing ionic size of R: (1) for the largest ionic size class (Nd in size 1.11 Å), four types (R-4Pr, R-3Pr, R-2Pr-a and R-2Pr-s) take part in the cell conversion; (2) for the second largest size class (Eu, Sm in size 1.07, 1.08 Å), three types (R-4Pr, R-3Pr, R-2Pr-a) take part in; (3) for the third class (Gd in size 1.05 Å), two types (R-4Pr, R-3Pr) take part in; and (4) for the fourth class (Y, Ho, Dy in size 1.02–1.03 Å), as described in Sec. II, the relevant configurations are R-4Pr and Pr-4R. These configurations are assigned in Table I according to the ionic sizes.

Figure 5 exhibits a result of the computer simulation for (a) the original site-percolation structure with x=0.319 and (b) the corresponding structure modified by the cell conversion, in which the configurations R-4Pr, R-3Pr, R-2Pr-a, and R-2Pr-s take part. These converted R cells (gray squares) join Pr cells (black squares) to construct the nonsuperconducting cluster throughout the system, creating a virtual threshold $x_2 \simeq 0.3$ much lower than the original one x_{pc2} =0.59.

Let us estimate the values of x_2 and x_1 for the converted percolation system with Pr concentration x. The concentration (N_n) of the isolated R cells, each of which adjoins nPr cells as denoted by R-nPr, is given by

$$N_n = C_n(1-x)^{5-n}x^n \quad (4 \geqslant n \geqslant 1), \tag{4}$$

where C_4=1, C_3=C_1=4, and C_2=6. If these centered R cells are converted, then the virtual thresholds x_2 and x_1 are approximately given by the solutions of the following equation:

$$x + \sum_{n=1}^{4} k_n N_n = x_{pc}, \tag{5}$$

where the original percolation threshold x_{pc}=x_{pc2} or x_{pc1}, and the coefficient k_n stands for a contribution weight of the configuration R-nPr to the cell conversion, and takes a value such that k_4=1, k_3=1 or 0, k_2=1, 2/3 (asymmetric), 1/3 (symmetric), or 0, according to the easiness for the cell conversion. We assume here that the configuration R-1Pr does not contribute to the cell conversion, and hence put k_1=0. As shown in Table I, with increasing ionic size of R, the cell conversion becomes easy, that is, the number of effective k_n's ($\neq$0) increases. It should be stressed again that the solutions of Eq. (5) are approximate to the real values of x_2 and x_1, because the percolation system suffering the cell conversion loses more or less completeness in its structural randomness.

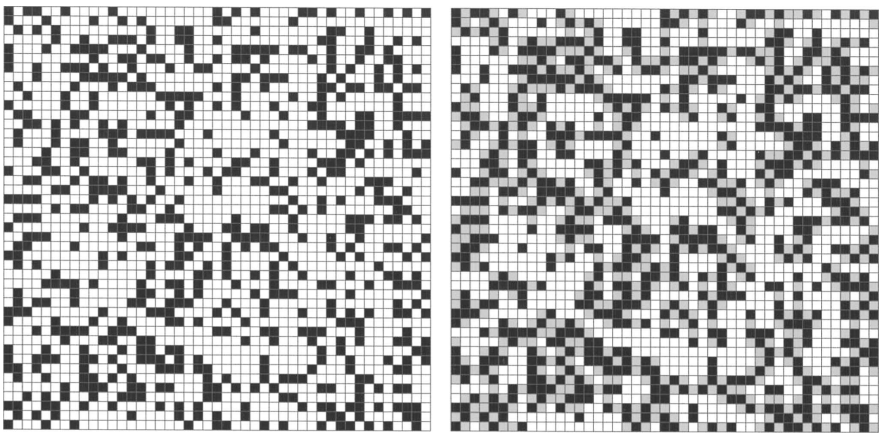

FIG. 5. (a) The initial site-percolation structure of the square lattice (RPr-123 with x=0.319), and (b) the corresponding percolation structure of class 1 involving cell conversion by R-4Pr, R-3Pr, R-2Pr-a, R-2Pr-s, where R cells are denoted by white squares, Pr cells by black squares, and the cells converted from R cells by gray squares; periodic boundary condition is applied.

In Table I, the values for x_2 and x_1 are given from experimental observations, the calculation, and the computer simulation; the system simulated has a size $L^2=10^4$. These values are classified into four classes according to the ionic sizes, as described above. The experimental values of the critical concentration x_2 were obtained from the literature showing x at which the zero-resistance temperature begins to disappear. The values of x_2 calculated from Eq. (5) approximate to the experimental ones. Better agreement is seen for the simulated values of x_2. As for x_1, the experimental value has been obtained for YPr-123 alone.[16] Although x_1 is to be observed also for other classes of *R*Pr-123, its appearance would not be so sharp in comparison with that for YPr-123, since the structural inhomogeneity is enhanced for *R*Pr-123 having large ionic size of *R*. For class 3, the simulated value of x_1 is just equal to the classical threshold x_{c1}, because the cell conversions due to *R*-3Pr and *R*-4Pr give no change in constructing the current path of type 1 as depicted in Fig. 1(a). Equation (5) does not take account of such geometrical effects of the cell configuration, and therefore its calculation underestimates more or less the value of x_1.

In spite of the above agreement between the model and the experimental observations, an exception remains when the ionic size of R^{3+} is considerably smaller than that of Pr^{3+} (its ionic radius=1.13 Å in eightfold configuration) as is typically seen for YbPr-123 (ionic radius of Yb^{3+}=0.98 Å in eightfold configuration). The value of x_2 at which S-I transition occurs has been found to be as high as the original threshold $x_{pc2}=0.59$ or more; for YbPr-123, x_2 has been observed to range from 0.59 (Ref. 34) to 0.65 (Ref. 35). This case may be categorized as class 5. The exception as observed for YbPr-123 will reflect the following situation. For such a large difference between ionic sizes of Pr and *R*, violation of the structural randomness will no longer be trivial, that is, the solid solution of Pr and *R* cells will become structurally incomplete, forming an asymmetric percolation structure. Probably, in this situation, the Pr cells will tend to prefer other Pr cells on joining and have a tendency of weak aggregation, while *R* cells will tend to form a continuous phase, for which the conversion of the isolated *R* cell will become less frequent. This tendency will lead the percolation threshold x_2 to become high.

The present percolation model describes well the S-I transition observed for the doped family of *R*Pr-123. However, the model will not straightforwardly be applied to other types of cuprates, since those cuprates have more complicated crystal structures, and various aspects other than considered in the present model should be taken into account. For example, the family of $RBa_2Cu_4O_8$ (*R*-124) is structurally rather close to *R*-123, but has the highly conducting double Cu-O chains and its conduction exhibits three-dimensional characteristics rather than 2D ones at low temperatures.[36] In addition, the T_c itself markedly depends (ranges from 57 to 81 K) on the ionic size of *R*.[37] Furthermore, a striking contrast is that Pr-124 itself becomes metallic (though not superconducting) at low temperatures (below about 150 K).[38] Therefore, the nanometric mixture (*R*Pr-124) consisting of *R*-124 and Pr-124 will exhibit more complicated transport behavior than that of *R*Pr-123.

In the present model, the 4*f* orbital of *R* in the converted *R* cell adjoining the Pr cells is assumed to hybridize with 2*p* of O in the CuO_2 plane. With the aid of this hybridization, the magnetic moment of the R^{3+} in the converted cell will also take part in the superexchange interaction with neighboring Pr^{3+} (or such converted R^{3+}) via the oxygen [*R*-O-Pr(*R*)], and thereby substantially contribute to the spatial spread of the antiferromagnetic ordering with respect to Pr^{3+}. Therefore, the critical concentration x_N(Pr) for the magnetic ordering at which Néel temperature T_N(Pr) begins to rise will also decrease with decreasing x_2.

IV. SUMMARY

The ionic size effect on the S-I transition in *R*Pr-123 has been investigated in terms of the nonclassical percolation process. In this process, the unit cell of *R*-123 can be converted with the aid of 4*f*-2*p* hybridization on contacting Pr cells into a different cell behaving as if it were a Pr cell. The converted *R* cells are substantially counted as Pr cells, thereby reducing the percolation threshold x_2 which refers to the S-I transition point. This virtual percolation threshold x_2, which originates from the classical threshold x_{pc2}, is quantitatively determined from this percolation process by considering several types of configurations for the cell conversion. The conversion becomes easy as the ionic size of *R* increases, giving the size effect. The ionic size dependence of the S-I transition derived from this model agrees well with experimental observations. The present model will be the first that can quantitatively determine the S-I transition point x_2 for a series of *R*Pr-123. Another virtual threshold x_1 is also yielded by the cell conversion from the classical threshold x_{pc1}. The model describes also that the conversion of *R* cells induces a spatial spread of the Pr^{3+}-type magnetic ordering by involving spins of R^{3+} in the converted cells.

ACKNOWLEDGMENTS

The author is grateful to T. Goya (currently at Okinawa Electric Power Co., Inc.) for his help in the experiment, and also to M. Matsukawa at Iwate University for his encouragement during the course of the work.

[1] H. D. Yang, P. F. Chen, C. R. Hsu, C. W. Lee, C. L. Li, and C. C. Peng, Phys. Rev. B **43**, 10568 (1991).
[2] Y. Xu and W. Guan, Appl. Phys. Lett. **59**, 2183 (1991).
[3] Y. Xu and W. Guan, Phys. Rev. B **45**, 3176 (1992).
[4] S. K. Malik, C. V. Tomy, and P. Bhargava, Phys. Rev. B **44**, 7042 (1991).
[5] J. Fink, N. Nücker, H. Romberg, M. Alexander, M. B. Maple, J. J. Neumeier, and J. W. Allen, Phys. Rev. B **42**, 4823 (1990).
[6] H. D. Jostarndt, U. Walter, J. Harnischmacher, J. Kalenborn, A. Severing, and E. Holland-Moritz, Phys. Rev. B **46**, 14872

(1992).
[7] R. Fehrenbacher and T. M. Rice, Phys. Rev. Lett. **70**, 3471 (1993).
[8] A. I. Liechtenstein and I. I. Mazin, Phys. Rev. Lett. **74**, 1000 (1995).
[9] A. V. Narlikar, A. Gupta, S. B. Samanta, C. Chen, Y. Hu, F. Wondre, B. M. Wanklyn, and J. W. Hodby, Philos. Mag. B **79**, 717 (1999).
[10] R. P. S. M. Lobo, E. Ya. Sherman, D. Racah, Y. Dagan, and N. Bontemps, Phys. Rev. B **65**, 104509 (2002).
[11] L. M. Paulius, C. C. Almasan, and M. B. Maple, Phys. Rev. B **47**, 11627 (1993).
[12] T. Harada and K. Yoshida, Physica C **383**, 48 (2002).
[13] L. Govea, R. Escudero, D. Rios-Jara, C. Piña, F. Morales, C. Wang, and R. A. Barrio, Physica C **153-155**, 940 (1988).
[14] C. Infante, M. K. El Mously, R. Dayal, M. Husain, S. A. Siddiqi, and P. Ganguly, Physica C **167**, 640 (1990).
[15] M. Muroi and R. Street, Physica C **216**, 345 (1993).
[16] K. Yoshida, Phys. Rev. B **60**, 9325 (1999).
[17] K. Yoshida and T. Hayasaka, Supercond. Sci. Technol. **15**, 1133 (2002).
[18] K. Yoshida and K. Ota, J. Phys.: Conf. Ser. **43**, 413 (2006).
[19] K. Yoshida, Physica B **284-288**, 644 (2000).
[20] K. Yoshida, T. Harada, and E. Kojima, Supercond. Sci. Technol. **16**, 720 (2003).
[21] In such doped samples the deterioration of the superconductivity inside the grain due to the Pr doping is more serious than that due to the grain boundary (except for extremely low x), and therefore the influence from the grain boundary will be concealed in the relative intensity in χ and ρ when depending on x (Ref. 17).
[22] For example, D. Stauffer and A. Aharony, *Introduction to Percolation Theory*, 2nd ed. (Taylor Francis, London, 1992), Chap. 2.
[23] Z. Tomkowicz, Physica C **320**, 173 (1999).
[24] X. W. Cao, C. Y. Wu, and J. C. Ho, Physica C **182**, 153 (1991).
[25] V. P. S. Awana, C. A. Cardoso, O. F. de Lima, R. Singh, A. V. Narlikar, W. B. Yelon, and S. K. Malik, Physica C **316**, 113 (1999).
[26] L. Colonescu, J. Berthon, R. Suryanarayanan, and I. Zelenay, Physica C **291**, 85 (1997).
[27] Z. Yamani and M. Akhavan, Phys. Status Solidi A **163**, 157 (1997).
[28] G. Cao, Y. Qian, X. Li, H. Wu, Z. Chen, and Y. Zhang, Physica C **248**, 92 (1995).
[29] J. J. Neumeier and M. B. Maple, Physica C **191**, 158 (1992).
[30] K. Latka, A. Szytula, Z. Tomkowicz, A. Zygmunt, and R. Duraj, Physica C **171**, 287 (1990).
[31] G. Nieva, S. Ghamaty, B. W. Lee, M. B. Maple, and I. K. Schuller, Phys. Rev. B **44**, 6999 (1991).
[32] W. Y. Guan, Y. C. Chen, J. Y. T. Wei, Y. H. Xu, and M. K. Wu, Physica C **209**, 19 (1993).
[33] The values here for Sm were estimated by the present author from the experimental data in Refs. 4 and 32.
[34] M. S. Hegde, X. Q. Xu, J. L. Peng, H. Zhang, R. L. Greene, and S. M. Green, Physica C **229**, 239 (1994).
[35] A. Gupta, H. Narayan, P. N. Lisboa-Filho, C. A. Cardoso, F. M. A. Moreira, O. F. De Lima, and A. V. Narlikar, Mod. Phys. Lett. B **16**, 261 (2002).
[36] N. E. Hussey, K. Nozawa, H. Takagi, S. Adachi, and K. Tanabe, Phys. Rev. B **56**, R11423 (1997).
[37] D. E. Morris, J. H. Nickel, J. Y. T. Wei, N. G. Asmar, J. S. Scott, U. M. Scheven, C. T. Hultgren, A. G. Markelz, J. E. Post, P. J. Heaney, D. R. Veblen, and R. M. Hazen, Phys. Rev. B **39**, 7347 (1989).
[38] N. Seiji, S. Adachi, and H. Yamauchi, Physica C **227**, 377 (1994).